Catalysis Letters 51 (1998) 85–93

Characterization of pure and sulfided $NiMoO_4$ catalysts using synchrotron-based X-ray absorption spectroscopy (XAS) and temperature-programmed reduction (TPR)

Sanjay Chaturvedi [a], José A. Rodriguez [a,*] and Joaquín L. Brito [b]

[a] *Department of Chemistry, Brookhaven National Laboratory, Upton, NY 11973, USA*
E-mail: rodrigez@bnl.gov

[b] *Centro de Química, Instituto Venezolano de Investigaciones Científicas (IVIC), Caracas 1020-A, Venezuela*

Received 11 November 1997; accepted 29 January 1998

This study aims at characterizing the properties of pure and sulfided $NiMoO_4$ catalysts using synchrotron-based near-edge X-ray absorption fine structure (NEXAFS) and temperature-programmed reduction (TPR). Mo L_{II}-edge and M_{III}-edge NEXAFS spectra indicate that on reaction with H_2S, the Mo component of $NiMoO_4$ gets partially reduced with the formation of MoS_2 type species. For the β-phase of $NiMoO_4$, the sulfidation of Mo is more extensive than for the α-phase, making the former a better precursor for catalysts of hydrodesulfurization (HDS) reactions. The Ni L_{II}-edge features are relatively insensitive to the changes accompanying the partial sulfidation of $NiMoO_4$. The sulfidation of the Ni component is confirmed by analysis of the Ni K-edge extended X-ray absorption fine structure (EXAFS) spectra which show the formation of Ni–S bonds (bond length $\sim$2.48 Å) and a $NiMoS_x$ phase. The S K-edge NEXAFS spectra show the presence of at least two types of sulfur species, one associated with a formal oxidation state of $2-$ and another associated with a formal oxidation state of $6+$. We attribute the former to the presence of metal–sulfur bonds (MoS_x and NiS_y). The latter is associated with the formation of S–O bonds (SO_4^{2-}). The formation of sulfates is also supported by the O K-edge NEXAFS spectra. The partially sulfided $NiMoO_4$ catalysts (both α- and β-isomorphs) have a much lower thermal stability in a reducing environment than pure $NiMoO_4$ and MoS_2. The sulfided molybdates react with H_2 in TPR producing H_2O and H_2S at temperatures above 400 K.

Keywords: nickel molybdate, HDS catalysts, sulfur poisoning, X-ray absorption spectroscopy

1. Introduction

Under atmospheric pressure, three phases of $NiMoO_4$ stoichiometry can exist, usually designated as α, β and the hydrate [1–3]. In all three compounds, Ni^{2+} ions occupy sites with octahedral coordination. The coordination of Mo^{6+} ions is octahedral in the α-phase while it is tetrahedral in both the β- as well as the hydrate-phase [4]. Nickel molybdates are important components of the industrial catalysts used for the partial oxidation of hydrocarbons [5]. These catalysts are very sensitive to sulfur poisoning and it is important to understand how the reaction with H_2S affects the properties of these mixed metal oxide catalysts. In addition, molybdates of the type $NiMoO_4$ have been detected several times in the industrial catalysts (Ni–Mo/Al_2O_3) used for hydrodesulfurization processes [6,7]. Prior work has shown that sulfided β-$NiMoO_4$ is a much better catalyst for the hydrodesulfurization (HDS) of thiophene than sulfided α-$NiMoO_4$ [8–10]. This study is aimed at characterizing the electronic and chemical properties of $NiMoO_4$ catalysts both, before and after sulfidation, using X-ray absorption spectroscopy (XAS) and temperature-programmed reduction (TPR).

NEXAFS performed with synchrotron radiation has emerged as a very powerful tool for characterizing the electronic properties of catalytic materials [11]. Recent works have shown that the local site symmetry of molybdenum oxide phases dispersed on MgO, TiO_2, Al_2O_3 and SiO_2 can be determined using the Mo $L_{II,III}$-edges [12,13]. These edges are due to $2p \rightarrow 4d$ electronic transitions and the variable splitting in the Mo $L_{II,III}$-edges reflects the ligand field splitting of the d orbitals. Also, the Mo M-edges are very sensitive to the oxidation state of Mo and a measurement of the energy position of the peak center of the Mo M_{III}-edge feature can be used to identify the oxidation state of Mo [14,15]. A similar measurement of the Ni L_{III}-edge can yield information about the oxidation state of Ni [14,16]. The results of the metal M- and L-edges often provide either additional or complementary information to the O K-edge measurements of the transition metal oxides [14]. There is a direct relation between the features in the O K-edge spectrum and the number of electrons in the d metal [17,18]. Several studies have demonstrated that the leading edge position of the S K-edge feature depends very strongly on the oxidation state of sulfur in a compound [14,21–24]. Finally, Ni K-edge extended X-ray absorption fine structure (EXAFS) spectroscopy has been used to accurately determine the structural parameters of nickel oxide systems [19,20]. Thus, a measurement of the Mo L- and M-edges, Ni K- and L-edges, O K-edge and S K-edge spectra should pro-

* To whom correspondence should be addressed.

vide detailed information about the structural and electronic properties of pure and sulfided $NiMoO_4$ catalysts. In addition, these spectra can be used as "fingerprints" to detect the presence of these compounds in supported catalysts.

2. Experimental

$NiMoO_4$ samples were prepared following the methodology described in detail in [8,9,25]. Both α- and β-$NiMoO_4$ were synthesized from the hydrated sample which was prepared by coprecipitation from aqueous $Ni(NO_3)_2$ and ammonium heptamolybdate [9,26]. The α-phase was prepared by firing H_2O–$NiMoO_4$ at 550 °C and slowly cooling to room temperature ($\sim$5 °C/min). The β-isomorph was prepared in a similar manner except that the temperature was always kept above 300 °C to avoid the formation of the α-isomorph [4,8,9]. The samples were partially sulfided by passing the same amount of H_2S through the α- and the β-isomorphs at 400 °C in a U tube quartz reactor.

The Mo $L_{II,III}$-edge and S K-edge NEXAFS spectra were recorded at the NSLS on beamline X-19A. The beamline is equipped with a boomerang-type flat crystal monochromator with Si(111) crystals. The harmonic content was reduced by detuning the monochromator by $\sim$90%. The measurements were performed in the "fluorescence-yield mode" using a Stern–Heald–Lytle detector with He as the detector gas [27,28].

The Ni L-edge, Mo M-edge and O K-edge NEXAFS spectra were acquired at the NSLS on beamline U-7A. This beamline is equipped with a toroidal–spherical grating monochromator. All spectra were acquired at room temperature in the "electron-yield mode" using a channeltron multiplier located near the sample surface [29a].

The Ni K-edge EXAFS spectra were taken at the NSLS on beamline X-6A. All these spectra were acquired in the transmission mode. The EXAFS oscillations were separated from the absorption background by using a cubic spline background removal technique [29b]. A k^3-weighted Fourier transform was applied to the EXAFS signal [29b] to obtain the Ni–O and Ni–S bond lengths.

The temperature-programmed reduction (TPR) experiments were performed in a RXM-100 instrument from Advanced Scientific Designs, Inc. The temperature of the sample was raised from 40 to 700 °C using a heating rate of 20 °C/min. The reduction was carried out in a gas flow that consisted of 15% H_2 + 85% N_2. The total flow rate was 50 ml/min. Chemical analysis of the desorbing products was performed using a quadrupole mass spectrometer (UTI 100C).

3. Results

The left panel of figure 1 shows the Mo L_{II}-edge NEXAFS spectra for a series of pure and sulfided molybdates. The corresponding features for two reference compounds (MoS_2 and MoO_3) are also included as the top and the bottom curves, respectively. All these spectra were acquired at room temperature. This edge probes 2p $\rightarrow$ 4d electronic transitions. The splitting in the Mo L_{II}-edge feature reflects the splitting of the 4d orbitals [4,12,30]: e and t_2 in T_d symmetry; t_{2g} and e_g in O_h symmetry. It can be seen that MoO_3 and α-$NiMoO_4$ show a splitting of 3.2 and 3.1 eV, respectively, while the splitting for H_2O–$NiMoO_4$ is $\sim$1.6 eV. In tetrahedral coordination, the splitting of the Mo 4d orbitals is smaller than the splitting in an octahedral coordination [4,12,30]. On this basis, we conclude that Mo is in an octahedral coordination in the α-isomorph while it is in a tetrahedral environment in the hydrate sample. A tetrahedral environment (Mo 4d splitting $<$2 eV) is also expected for β-$NiMoO_4$ [1–4], but this phase transforms into α-$NiMoO_4$ at the temperature at which the spectra in figure 1 were taken (25 °C). The sulfided samples of both the α- and β-$NiMoO_4$ show a line shape that is similar to the one obtained for MoS_2. The oxidation state of Mo is 4+ in MoS_2 compared to a value of 6+ for the oxides. MoS_2 has a trigonal prism structure [31]. When a trigonal perturbation is applied to d orbitals, there is scrambling of the t_{2g} and e_g orbitals resulting in loss of the discrete levels present in T_d or O_h environments [32]. This accounts for the single broad feature that we observe between 2624 and 2631 eV for the Mo L_{II}-edge NEXAFS spectrum of MoS_2. The similarity in the line shape of α-$NiMoO_4$ with MoO_3 suggests that Mo has a similar bonding environment in both compounds, while a comparison of the line shape of the sulfided samples with MoS_2 is indicative of the fact that Mo has a similar bonding environment in all three compounds.

The Mo L_{II}-edge peak position for MoS_2 is $\sim$2.0 eV lower than the corresponding position for the MoO_3 L_{II}-edge peak. The peak positions of the metal L-edge features are related to the formal oxidation state of the parent metal [14,33]. The formal oxidation state of Mo is 6+ in MoO_3 while it is 4+ in MoS_2. Both α- and H_2O–$NiMoO_4$ have the same L_{II}-edge peak positions as MoO_3 while the peak positions for the sulfided samples are lower than the value for MoO_3 but $\sim$1.0 eV higher than the value for MoS_2 ($MoS_2 < \beta$-$NiMoO_4$+S $< \alpha$-$NiMoO_4$+S $< MoO_3$). This indicates that Mo gets partially reduced upon sulfidation of $NiMoO_4$.

The Mo M_{III}-edge NEXAFS spectra are presented in the right panel of figure 1. This data supports the inferences drawn from the Mo L_{II}-edge spectra. The NEXAFS peak position for MoO_3 (bottom spectrum) is $\sim$1.2 eV higher than the corresponding position for MoS_2 (top spectrum) and the value for the sulfided $NiMoO_4$ samples lies in between the values for the two reference compounds (MoS_2 and MoO_3). Figure 2 shows the relationship between the main peak position in the Mo M_{III}-edge NEXAFS spectra and the Mo oxidation state. The data for Mo(110), O/Mo(110) and MoO_3 (obtained from [14] and [15]) denoted by circles lies on a straight line. A similar relationship between the peak position of the Ru M-edge feature and the oxidation state of Ru has been shown ear-

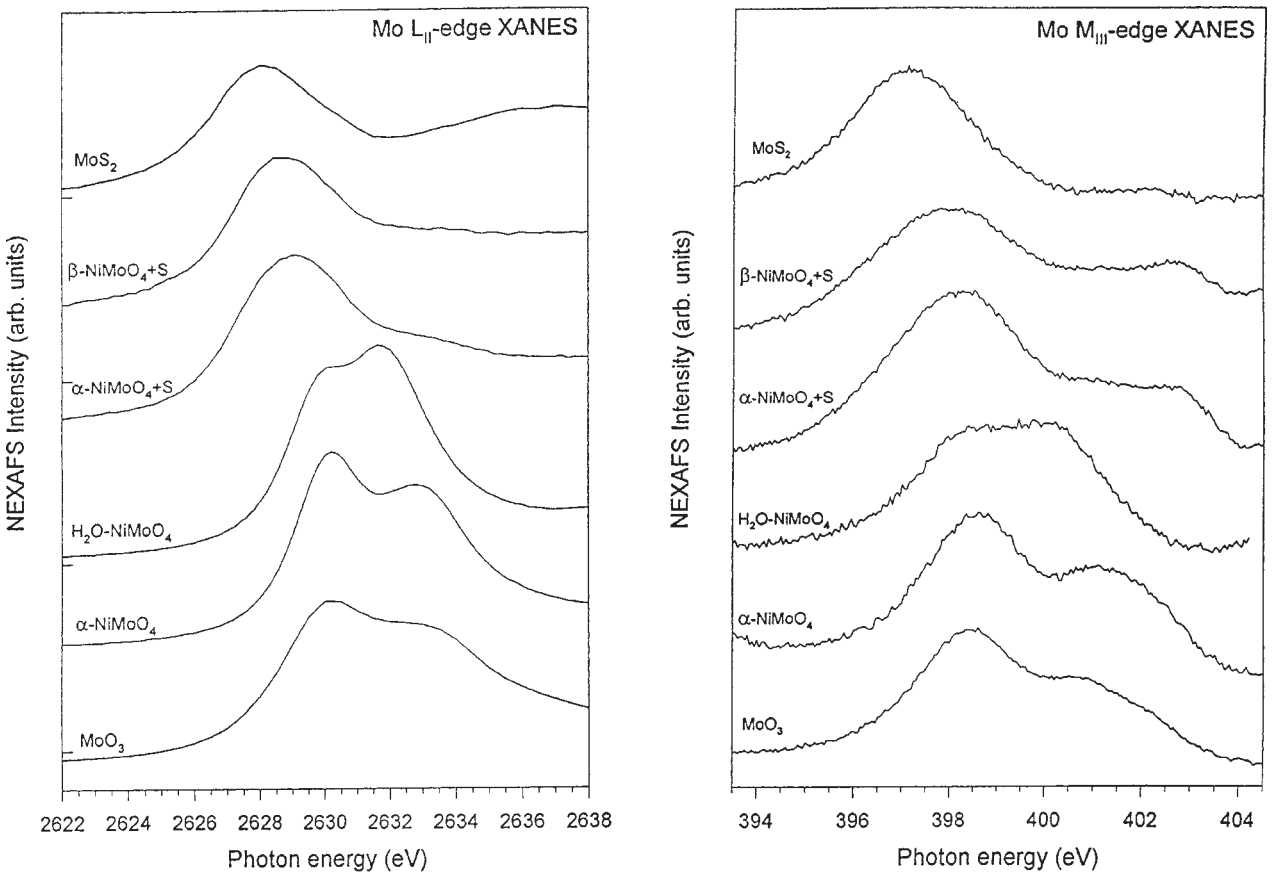

Figure 1. Left panel: Mo L_{II}-edge NEXAFS spectra of MoO_3, α-$NiMoO_4$, H_2O–$NiMoO_4$, α-$NiMoO_4$ (sulfided), β-$NiMoO_4$ (sulfided) and MoS_2. The splitting in the NEXAFS features reflects the d orbital splitting [12]. Right panel: Mo M_{III}-edge NEXAFS spectra of the same series of compounds shown in the left panel. All spectra were recorded at room temperature.

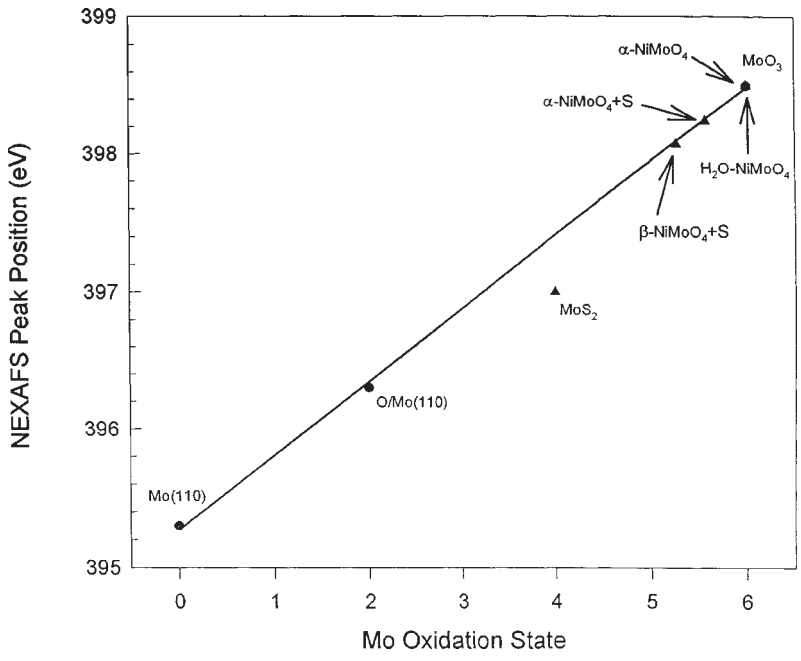

Figure 2. Plot of the Mo oxidation state versus the Mo M_{III}-edge NEXAFS peak position. The data for Mo(110), O/Mo(110) and MoO_3 (obtained from [14] and [15]) denoted by circles are fitted to a straight line ($r = 0.99$). The experimental data points for pure and sulfided $NiMoO_4$ samples are denoted by triangles that are set on the line at the measured NEXAFS peak positions. The value for MoS_2 is experimentally obtained and the point set at a formal oxidation state of 4+.

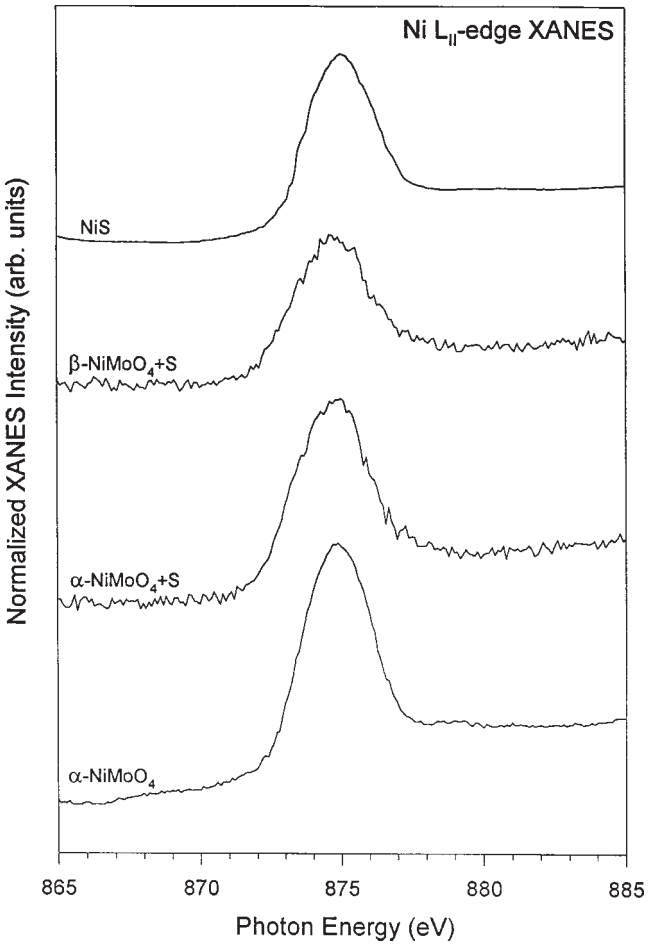

Figure 3. Ni L_{II}-edge NEXAFS spectra of α-$NiMoO_4$, α-$NiMoO_4$ (sulfided), β-$NiMoO_4$ (sulfided) and NiS.

lier [14,34]. The experimental data points are denoted by triangles that are fitted to the line. It can be seen that both α- and H_2O–$NiMoO_4$ coincide with MoO_3 indicating a formal oxidation state of 6+ for the Mo atom. The value for MoS_2 is experimentally obtained and the point set at a formal oxidation state of 4+. It can be seen that the NEXAFS peak positions for both sulfided $NiMoO_4$ samples are between the corresponding values for MoO_3 and MoS_2. This reinforces our previous contention that there is extensive sulfidation of Mo when both, α- and β-$NiMoO_4$ react with H_2S. Also, the peak positions indicate that on reaction with H_2S, β-$NiMoO_4$ is sulfided or reduced to a greater extent than the α-isomorph.

The Ni L_{II}-edge NEXAFS spectra for pure α-$NiMoO_4$ and the two sulfided samples are shown in figure 3. The spectrum for NiS is also included on the top for reference. This level probes the Ni(2p) $\rightarrow$ Ni(3d) electronic transition. There is no significant change in the NEXAFS peak position for α-$NiMoO_4$ on sulfidation. Sulfided β-$NiMoO_4$ also appears at the same energy position. Peak positions for NiO and H_2O–$NiMoO_4$ are $\sim$0.5 eV (not shown) lower than those shown in figure 3. These results indicate that the 3d orbitals of Ni are in a similar chemical environment in all the $NiMoO_4$ compounds. The concurrence of the peak position of NiS with the value for the three oxidic $NiMoO_4$ samples shown in the spectra suggests that the Ni L_{II}-peak position is not sensitive enough to see changes on sulfidation. The L-edge NEXAFS peak position for transition metals is known to be very sensitive to the oxidation state of the parent metal [14]. In this particular case, Ni is in 2+ oxidation state in all the compounds and this in part accounts for the relative insensitivity of the Ni L_{II}-edge to sulfidation. To address the issue of Ni sulfidation, we took Ni K-edge EXAFS data for both pure and sulfided $NiMoO_4$ samples.

The Ni K-edge probes primarily the Ni(1s) $\rightarrow$ Ni(4p) electronic transition while the pre-edge feature is associated with Ni(1s) $\rightarrow$ Ni(3d) electronic transition. This Ni(1s) $\rightarrow$ Ni(3d) pre-edge feature is symmetry forbidden in a strictly octahedral field but is allowed in a tetrahedral field. The complete absence of this feature in the Ni K-edge EXAFS of NiO, α-$NiMoO_4$+S and β-$NiMoO_4$+S (raw spectra not shown) suggests that Ni is in an octahedral environment in all the samples. Results obtained previously from EXAFS analysis of sulfided NiO–MoO_3 catalysts have shown that Ni is in an octahedral environment bonded to both oxygen as well as sulfur atoms [35]. The similarity of the sulfided systems suggests that it is possible that the $NiMoO_4$ phase exists in the NiO–MoO_3-supported catalysts. Figure 4 compares the Ni K-edge EXAFS results for α-$NiMoO_4$ (sulfided), β-$NiMoO_4$ (sulfided) and NiO. The figure shows the magnitude of the $k^3\chi(k)$ Fourier transform of the EXAFS spectra. In the top panel, the NiO data is used to calibrate the Ni–O bond length. The peak corresponding to the Ni–O bond length is set at a value of 2.08 Å [19,36a] and the peak at $\sim$3 Å is attributed to the Ni–Ni bond length [36b]. On similar treatment, the data for the sulfided samples of both α- and β-$NiMoO_4$ exhibit a peak corresponding to the Ni–O bond at $\sim$2.08 Å and an additional feature at 2.48 Å. This feature is absent in both NiO (top panel of figure 4) and α-$NiMoO_4$ (results not shown). We attribute this to the presence of Ni–S bonds. The corresponding value for bulk NiS [37] is reported to be between 2.33 and 2.39 Å. The higher value of the Ni–S bond length in our case may be in part due to the complex nature of the sulfided $NiMoO_4$ samples. Both sulfided samples also exhibit features between 2.7 and 2.8 Å. These match very well the Ni–Mo bond length that has been reported previously for $((C_6H_5)_4P)_2Ni(MoS_4)_2$ (2.79 Å) [36b] and Ni–MoS_2/C (2.82 Å) [38], and in our case, it is attributed to the Ni–Mo bond length in an amorphous $NiMoS_x$ phase formed upon sulfidation. Support for this argument comes from the absence of this feature in pure α-$NiMoO_4$ (results not shown). A small feature at $\sim$3.25 Å is assigned to the presence of Ni–Mo bonds in the $NiMoO_4$ that remains in the sample after sulfidation, since it was present in the case of pure α-$NiMoO_4$. Thus, the sulfided $NiMoO_4$ samples have the presence of both Ni–O and Ni–S bonds and on reaction with H_2S, Ni gets partially sulfided. We will come back to this point again when we describe the temperature-programed reduction (TPR) results. It may be argued that

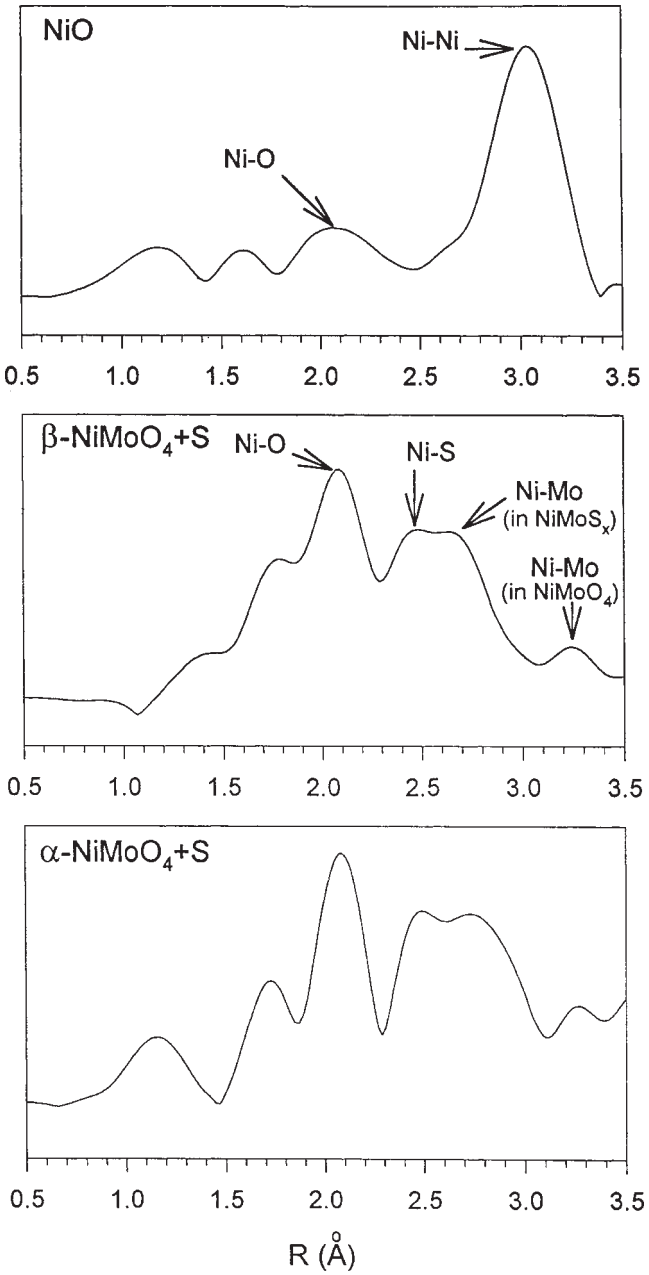

Figure 4. Plot of the magnitude of the Fourier transform of $k^3\chi(k)$ in the Ni K-edge EXAFS spectra for NiO, top panel, β-$NiMoO_4$ (sulfided), middle panel, and α-$NiMoO_4$ (sulfided), bottom panel. The NiO data is used to calibrate the Ni–O bond length and the peak corresponding to the Ni–O bond length is set at 2.08 Å. On similar treatment, the data for the sulfided samples of both α- and β-$NiMoO_4$ exhibits an additional feature at 2.48 Å that can be attributed to the presence of Ni–S bonds.

the samples picked up oxygen from atmosphere, but we ruled out this possibility by taking the Ni K-edge EXAFS spectra on samples that were sealed in an inert atmosphere after treatment with H_2S.

The S K-edge NEXAFS spectra of both α- and β-$NiMoO_4$ (sulfided) are exhibited in figure 5. Also shown for reference are the corresponding spectra for MoS_2 and a salt that contains a sulfate ($FeSO_4$). The S K-edge spectrum of MoS_2 is characterized by an intense edge at 2469.6 eV fol-

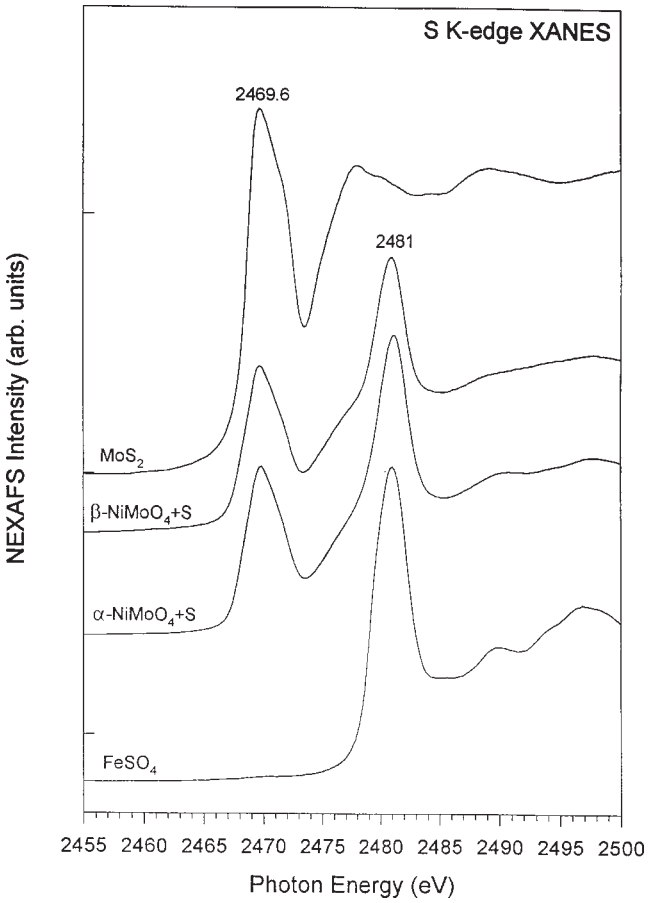

Figure 5. S K-edge NEXAFS spectra of MoS_2, α-$NiMoO_4$ (sulfided), β-$NiMoO_4$ (sulfided) and $FeSO_4$. All spectra were acquired at room temperature.

lowed by additional features at ∼2478 and ∼2488 eV. This is similar to the spectrum that has been reported previously for NiS [39]. Much of the structure observed in the NEXAFS spectra corresponds to transitions to bound states, although other phenomena such as shake-up and shake-down satellites and continuum resonances [24,39,40] also contribute. Bound state transitions commonly follow simple dipole selection rules, and an intense feature at the K-edge would thus be expected to correspond to a transition to a level possessing significant p-orbital character (e.g., $1s \rightarrow \pi^*$ or $1s \rightarrow \sigma^*$). Although, a detailed analysis of the NEXAFS spectra is beyond the scope of this work, we will aim at using the spectra to fingerprint the electronic nature of sulfur. We will focus our attention only on the NEXAFS peak position. The S K-edge for $FeSO_4$ occurs nearly 11 eV higher than the one for MoS_2. Both α- and β-$NiMoO_4$ (sulfided) samples show peaks at 2469.6 and 2481 eV. This suggests the presence of at least two kinds of sulfur species in the sample. The peak at lower photon energies is associated with the presence of metal sulfides (MoS_x and NiS) while the peak at higher photon energy (∼2481 eV) is associated with the formation of sulfate (SO_4^{2-}) species. We mentioned earlier that the samples were not fully sulfided (i.e., they still contain oxygen). Thus, it is not too sur-

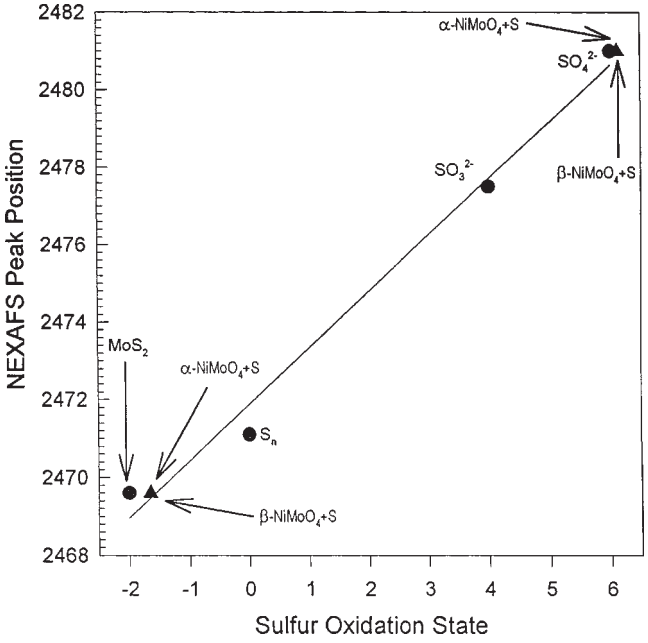

Figure 6. Plot of the sulfur oxidation state versus the S K-edge NEXAFS peak position. The values for the reference compounds (MoS_2, S_n, Na_2SO_3 and Na_2SO_4) are denoted by filled circles and the data is fitted to a straight line ($r = 0.99$). The values for α-$NiMoO_4$ (sulfided) and β-$NiMoO_4$ (sulfided) are denoted by triangles and set on the line. Both sulfided $NiMoO_4$ samples contain at least two different kinds of S species in two distinct oxidation states ($2-$ and $6+$). All the spectra were acquired at room temperature.

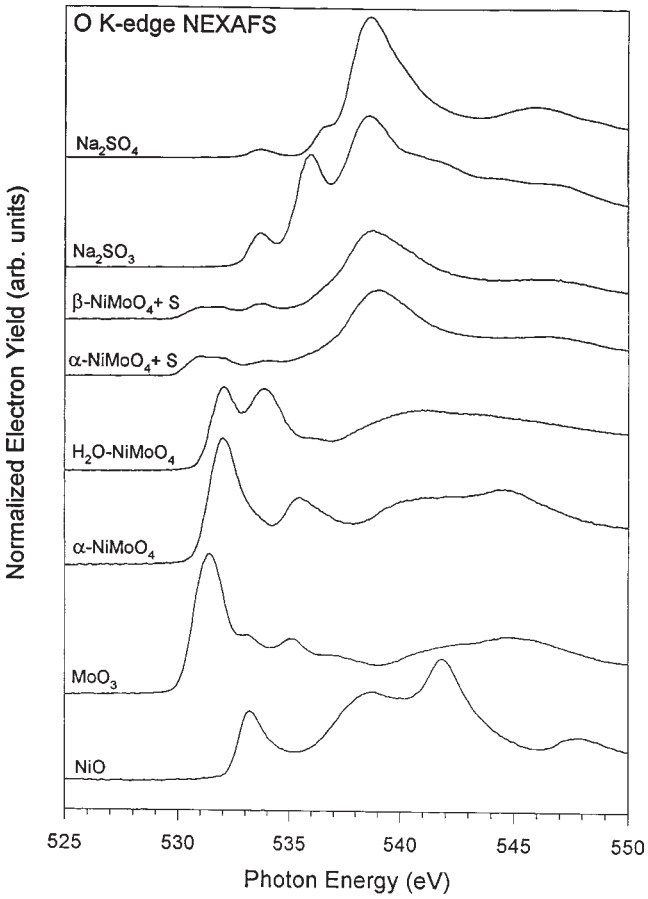

Figure 7. O K-edge NEXAFS spectra of MoO_3, α-$NiMoO_4$, H_2O–$NiMoO_4$, α-$NiMoO_4$ (sulfided), β-$NiMoO_4$ (sulfided), NiO, Na_2SO_3 and Na_2SO_4. All spectra were acquired at room temperature.

prising that the sulfur interacts with oxygen to form sulfate type species. The S K-edge NEXAFS spectrum of $FeSO_4$ shows additional features at ∼2490 and ∼2497 eV. These are associated with the SO_4^{2-} species and have also been reported earlier for both K_2SO_4 [24] and Na_2SO_4 [39]. The spectra for the two sulfided $NiMoO_4$ samples also show broad features in this region and offer additional proof for the presence of sulfate species. Further proof for the formation of sulfate is offered in the O K-edge spectra presented later in figure 7.

Several earlier studies have amply demonstrated that the peak position of the S K-edge NEXAFS spectra can be used to characterize the oxidation state of sulfur [14,21–24]. Figure 6 shows a plot of the sulfur oxidation state versus the NEXAFS peak position. The filled circles for MoS_2, S_n, SO_3^{2-} and SO_4^{2-} are the reference compounds (NEXAFS peak positions were obtained experimentally except for SO_3^{2-} which was taken from [39]) that correspond to a sulfur oxidation state of $2-$, 0, $4+$ and $6+$, respectively. The data were fitted (solid line) with a least squares line ($r = 0.99$). The energy positions of the two peaks in both α- and β-$NiMoO_4$ (sulfided) samples are indicated by triangles on the regression line. It can be clearly seen that there are at least two sulfur species present in each of the sulfided $NiMoO_4$ samples. The sulfur appearing at a photon energy of 2469.6 eV (oxidation state $\sim 1.7-$) is associated with the presence of metal–sulfur bonds that could be associated with MoS_x and NiS_y. The sulfur NEXAFS feature appearing at 2481 eV (oxidation state $\sim 6+$) is attributed to the presence of sulfur–oxygen bonds in sulfate species (SO_4^{2-} that are formed on the reaction H_2S with the $NiMoO_4$ catalysts.

Figure 7 shows the O K-edge NEXAFS spectra for α-$NiMoO_4$, H_2O–$NiMoO_4$ and sulfided α- and β-$NiMoO_4$. Also included in the figure are the spectra for a few reference compounds: MoO_3, NiO, Na_2SO_3 and Na_2SO_4. For metal oxides, the structure at the O K-edge arises from covalent mixing of the metal and oxygen states, which introduces O(2p) character in unoccupied states of mainly metal character making the O(1s) → metal(d,s,p) electronic transitions dipole allowed [16–18]. In the case of the $NiMoO_4$ system, one can have electronic transition from O(1s) orbitals to the empty orbitals of either Ni or Mo. Upon inspection, it can be seen that the line shape of the O K-edge spectrum of both α-$NiMoO_4$ and H_2O–$NiMoO_4$ bears closer resemblance to MoO_3 than to NiO. This indicates that the O(1s) electrons are excited primarily into the Mo(4d,5s,5p) orbitals. There are three reasons that could account for this behavior. First, the O(1s) → Mo(4d,5s,5p) transitions may occur at a lower energy than the O(1s) → Ni(3d,4s,4p) transitions. Second, the mixing of the O(2p) orbitals with the Mo(4d) orbitals is stronger than with the 3d orbitals of Ni making the O(s) → Mo(d) transition more dipole allowed than the O(1s) → Ni(d) transition. Finally, Mo^{6+}

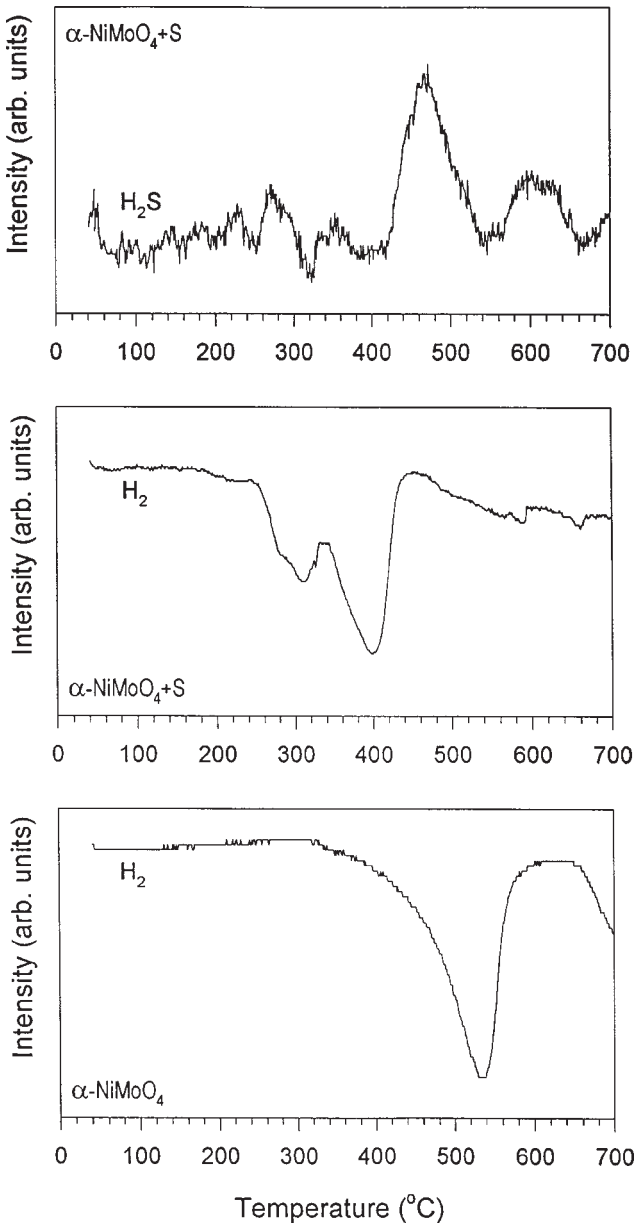

Figure 8. Top panel: H_2S evolution resulting from the H_2-TPR of α-$NiMoO_4$ (sulfided). Middle panel: H_2 consumption during the TPR of α-$NiMoO_4$ (sulfided). Bottom panel: H_2 consumption during the TPR of pure α-$NiMoO_4$.

has a fully empty valence d shell while the valence d shell of Ni^{2+} is more than half occupied. It has been shown in an earlier contribution [4] that the separation in the first and second peak in the O K-edge NEXAFS spectra tracks very well with the splitting in the Mo L_{III}- and L_{II}-edges and reflects changes in the magnitude of the splitting of the Mo(4d) orbitals when going from octahedral to tetrahedral coordination. The O K-edge NEXAFS spectra provide additional support to the data in figure 1 where we showed that the coordination of Mo is O_h in α-$NiMoO_4$ and T_d in H_2O–$NiMoO_4$. T_d coordination is also observed in the case of β-$NiMoO_4$ [8].

The case of the sulfided $NiMoO_4$ samples is quite complex because in addition to O(1s) $\rightarrow$ metal(d,s,p) electronic transitions, we can also have transitions from O(1s) $\rightarrow$ S(3d,4s,4p) orbitals. Qualitatively, the line shape of the O K-edge NEXAFS spectra of both sulfided $NiMoO_4$ samples is quite similar to that of Na_2SO_4 (note that the line shape of Na_2SO_3 is quite different). The main peak in all cases is centered at $\sim$538.5 eV. We attribute this to a O $\rightarrow$ S electronic transition. This suggests that in the sulfided $NiMoO_4$ samples, the oxygen is present as sulfates (SO_4^{2-}). The sulfided $NiMoO_4$ samples also show additional weak features between 530 and 535 eV. This is concurrent with the features seen for MoO_3 and NiO. Thus, some oxygen in the sulfided samples remains bonded to Mo or Ni.

We carried out temperature-programmed reduction (TPR) for a series of $NiMoO_4$ systems by heating the samples at 20 °C/min in a 50 cm^3/min flow of 15% $H_2 + 85\%$ N_2. For the sake of brevity, we present the results only for the pure and sulfided α-$NiMoO_4$. The hydrogen consumption for the TPR of pure α-$NiMoO_4$ (bottom panel of figure 8) shows a dip at $\sim$540 °C. Prior work comparing the reducibility of pure α-$NiMoO_4$ with pure β-$NiMoO_4$ has shown that the α-isomorph is reduced $\sim$60 °C lower than the corresponding value for the β-isomorph [8]. TPR of pure MoS_2 did not cause any change in the H_2 background and did not result in the evolution of H_2S either. The stability of MoS_2 in H_2 under atmospheric pressure at temperatures up to 800 °C has been well documented [41]. The top panel of figure 8 shows the evolution of H_2S when sulfided α-$NiMoO_4$ is reduced with hydrogen. There is a main peak centered at $\sim$475 °C indicating that the sulfur from the sample combines with the flowing H_2 to form H_2S. A look at the hydrogen consumption (middle panel of figure 8) reveals that the majority of the hydrogen is consumed between 250 and 450 °C. Water (not shown) desorbs as a broad feature in this temperature range. There is also a smaller consumption of hydrogen at 580 and 650 °C that results in the evolution of H_2S. Qualitatively, the hydrogen consumption for β-$NiMoO_4$ (sulfided) displayed similar behavior. Thus, the reduction of both α-$NiMoO_4$ (sulfided) and β-$NiMoO_4$ (sulfided) results in the evolution of H_2O and H_2S. This is conclusive evidence that the samples are only partially sulfided. All these results taken together show that both sulfided α- and β-$NiMoO_4$ are more easy to reduce than pure $NiMoO_4$ or MoS_2.

4. Discussion

Nickel molybdates used as catalysts in the partial oxidation of hydrocarbons [5] are very sensitive to sulfur poisoning. The Mo L- and M-edge NEXAFS results suggest that on reaction of $NiMoO_4$ with H_2S, the Mo gets reduced due to the formation of Mo–S species akin to MoS_2. It is interesting to note that MoS_x is formed from both α-$NiMoO_4$ (where Mo is in O_h coordination) and β-$NiMoO_4$ (where Mo is in T_d coordination). It has been reported in the literature that MoS_2 is readily formed by heating MoO_3 in H_2S [31]. We suspect a similar process occurs when

$NiMoO_4$ is heated in the presence of dihydrogen sulfide. Upon reaction with H_2S, the Ni atoms in both α- and β-$NiMoO_4$ are also partially sulfided and, in addition, there is formation of SO_4^{2-} species.

A prior study has shown that during the TPR of HDS catalysts prepared by sulfiding Ni–Mo/Al_2O_3 [42], there is reaction with H_2 between 250 and 350 °C. In our experiments, the sulfided $NiMoO_4$ samples show two peaks for H_2 consumption at 250 and 400 °C. The differences in the peak temperatures can be attributed to different experimental conditions and are also due to the sample differences (Ni–Mo/Al_2O_3 versus $NiMoO_4$). However, the similarity does suggest that a phase resembling sulfided $NiMoO_4$ may be present in industrial type Ni–Mo/Al_2O_3 catalysts and is a convenient precursor of the active HDS catalysts. In addition, the EXAFS data suggests that a compound that resembles sulfided $NiMoO_4$ is formed during the sulfidation of NiO–MoO_3 industrial-like catalysts. Furthermore, the EXAFS results for the sulfided $NiMoO_4$ samples show features similar to those seen in Ni–MoS_2/C catalysts [38], suggesting that a $NiMoS_x$ phase is formed after exposing the molybdates to H_2S. This $NiMoS_x$ phase could contain the Ni–Mo–S units that are proposed to be the active sites for HDS reactions on industrial catalysts [43].

It has been shown earlier that the thiophene HDS activity of sulfided β-$NiMoO_4$ is higher (20–40%) than that of sulfided α-$NiMoO_4$ [8–10]. This difference in catalytic activity cannot be attributed to variations in the surface areas of the sulfides derived from α- and β-$NiMoO_4$ [8,9]. Since the Ni EXAFS data does not show any significant differences in the two samples, we will try to explain this behavior by taking into account the properties of the Mo sites. The higher catalytic activity of the β-isomorph as compared to α-$NiMoO_4$ can be understood in terms of a higher number of catalytic sites on the former. A close inspection of the Mo L_{II}- and M_{III}-edge NEXAFS spectra of the two samples reveals that the sulfided β-isomorph is more closely related to MoS_2 than the α-isomorph. In the tetrahedral environment of the β-phase, a Mo^{6+} ion is coordinatively unsaturated and in overall its empty 4d orbitals are less destabilized than in an octahedral field [44]. This favors bonding interactions between the Mo(4d) orbitals and the sulfur lone pairs of H_2S. In other words, the β-$NiMoO_4$ (sulfided) is not as sulfur deficient as the corresponding α-isomorph in the precursor state. Therefore, under the HDS conditions, β-$NiMoO_4$ (sulfided) produces a greater number of active MoS_x or $NiMoS_x$ sites.

In a previous work [45], after comparing the sulfidation of MoO_3 and $Al_2(MoO_4)_3$, it has been proposed that octahedrally coordinated Mo^{6+} is more easily sulfided than tetrahedrally coordinated Mo^{6+}. A direct comparison of the results for MoO_3 versus $Al_2(MoO_4)_3$ and α- versus β-$NiMoO_4$ can be misleading. $Al_2(MoO_4)_3$ is more difficult to sulfide than MoO_3, but these compounds have very different crystalline structures. This is not the case for the two phases of $NiMoO_4$, where the basic structure is the same but for the coordination of Mo.

5. Conclusions

(1) The reaction of H_2S with both α-$NiMoO_4$ and β-$NiMoO_4$ results in extensive sulfidation of these compounds. The results of X-ray absorption spectroscopy (XAS) show the formation of MoS_x type species and the presence of both Ni–S bonds and Ni–O bonds. There are at least two kinds of sulfur species present in the sulfided $NiMoO_4$ samples. One is sulfur associated with the transition metals (MoS_x and NiS_y) and the other is sulfur associated with sulfate (SO_4^{2-}) species. The higher HDS catalytic activity of β-$NiMoO_4$ (sulfided) compared to the α-$NiMoO_4$ (sulfided) may be related to a more extensive sulfidation of Mo in the former that leads to a greater number of catalytic sites.

(2) Reduction of the sulfided $NiMoO_4$ samples occurs at lower temperatures than those for either of the pure phases and results in the evolution of H_2O and H_2S. A comparison of the TPR and EXAFS results with those obtained for other relevant systems indicates that sulfided $NiMoO_4$ (which contains a $NiMoS_x$ phase) may be present in the sulfided samples of both NiO/MoO_3 and Ni–Mo/Al_2O_3 industrial catalysts.

(3) Our results show that NEXAFS is a very powerful technique to study the interaction of sulfur and molybdenum-oxide catalysts. It allows the determination of the oxidation states of S and Mo and the characterization of these complex catalytic systems (see figures 2 and 6).

Acknowledgement

The authors would like to thank D.A. Fischer, F.L. Lu and P. Lee for their help with the use of the U7A, X19A and X6A beamlines, respectively, at the NSLS. The NSLS is supported by the divisions of Materials and Chemical Sciences of the US Department of Energy. The work was carried out at the Chemistry Department of BNL and was supported under contract DE-AC02-76CH00016 with the US Department of Energy, Office of Basic Energy Sciences, Chemical Science Division.

References

[1] G.W. Smith and J.A. Ibers, Acta Cryst. 19 (1965) 269.
[2] G.W. Smith, Acta Cryst. 15 (1962) 1054.
[3] A.W. Sleight and B.L. Chamberlain, Inorg. Chem. 7 (1968) 1673.
[4] J.A. Rodriguez, S. Chaturvedi, J.C. Hanson, A. Albornoz and J.L. Brito, J. Phys. Chem. B 102 (1998), in press.
[5] J. Zou and G.L. Schrader, J. Catal. 161 (1996) 667.
[6] J.L. Brito and J. Laine, Appl. Catal. 72 (1991) L13 and references therein.
[7] R.A. Madeley and S.E. Wanke, Appl. Catal. 39 (1988) 295.
[8] J.L. Brito, A.L. Barbosa, A. Albornoz, F. Severino and J. Laine, Catal. Lett. 26 (1994) 329.
[9] J.L. Brito and A.L. Barbosa, J. Catal. 171 (1997) 467.
[10] J. Laine and K.C. Pratt, React. Kinet. Catal. Lett. 10 (1979) 207.
[11] A.P. Hitchcock and D.C. Mancini, J. Electron. Spectrosc. Related Phenom. 67 (1994) 1 and references therein.

[12] S.R. Bare, G.E. Mitchell, J.J. Maj, G.E. Vrieland and J.L. Gland, J. Phys. Chem. 97 (1993) 6048.
[13] H. Hu, I.E. Wachs and S.R. Bare, J. Phys. Chem. 99 (1995) 10,897.
[14] J.G. Chen, Surf. Sci. Reports 30 (1997) 1.
[15] J.G. Chen, Chem. Rev. 96 (1996) 1477.
[16] J.G. Chen, B. Frühberger and M.L. Colaianni, J. Vac. Sci. Technol. A 14 (1996) 1668.
[17] F.M.F. de Groot, M. Grioni, J.C. Fuggle, J. Ghijsen, G.A. Sawatzky and H. Petersen, Phys. Rev. B 40 (1989) 5715.
[18] L.A. Grunes, R.D. Leapman, C.N. Wilker, R. Hoffmann and A.B. Kunz, Phys. Rev. B 25 (1982) 7157.
[19] K.I. Pandya, W.E. O'Grady, D.A. Corrigan, J. McBreen and R.W. Hoffman, J. Phys. Chem. 94 (1990) 21.
[20] J. McBreen, W.E. O'Grady, K.I. Pandya, R.W. Hoffman and D.E. Sayers, Langmuir 3 (1987) 428.
[21] A. Vairavamurthy, B. Manowitz, G.W. Luther III and Y. Jeon, Geochim. Cosmochim. Acta 57 (1993) 1619.
[22] M.J. Morra, S.E. Fendorf and P.D. Brown, Geochim. Cosmochim. Acta 61 (1997) 683.
[23] P. Frank, B. Hedman, R.M.K. Carlson, T.A. Tyson, A.L. Roe and K.O. Hodgson, Biochemistry 26 (1987) 4975.
[24] G.N. George and M.L. Gorbaty, J. Am. Chem. Soc. 111 (1989) 3182.
[25] J.L. Brito, J. Laine and K.C. Pratt, J. Mater. Sci. 24 (1989) 425.
[26] C. Mazzochia, F. Di Renzo and P. Centola, Rev. Port. Quim. 19 (1977) 61.
[27] E. Stern and S. Heald, Rev. Sci. Instrum. 50 (1979) 1579.
[28] F.W. Lytle, R.B. Greegor, D.R. Sandstrom, E.C. Marques, J. Wong, C.L. Spiro, G.P. Huffman and F.E. Huggins, Nucl. Instrum. Methods Phys. Res. 226 (1984) 542.
[29] (a) D.A. Fischer, in preparation;
(b) M.J. Fay, A. Proctor, D.P. Hoffmann and D.M. Hercules, Anal. Chem. 60 (1988) 1225A.
[30] B. Hedman, J.E. Penner-Hahn and K.O. Hodgson, in: *EXAFS and Near Edge Structure*, eds. K.O. Hodgson, B. Hedman and J.E. Penner-Hahn (Springer, Berlin, 1984).
[31] F.A. Cotton and G. Wilkinson, *Advanced Inorganic Chemistry*, 5th Ed. (Wiley, New York, 1988).
[32] C.J. Ballhausen, *Introduction to Ligand Field Theory* (McGraw-Hill, New York, 1962).
[33] J. Tafto and O.K. Krivanek, Phys. Rev. Lett. 48 (1982) 560.
[34] S.P. Kelty, J.G. Chen, A.F. Ruppert, R.R. Chianelli, J. Ren and M.H. Whangbo, Surf. Sci., submitted.
[35] A. Clozza, A. Bianconi, J. Garcia, A. Corma and E. Burattini, Physica B 158 (1989) 162.
[36] (a) P. Mahto and A.R. Chetal, Phys. Rev. Lett. 58 (1987) 889;
(b) S.M.A.M. Bouwens, J.A.R. van Veen, D.C. Koningsberger, V.H.J. de Beer and R. Prins, J. Phys. Chem. 95 (1991) 123.
[37] J. Trahan, R.G. Goodrich and S.F. Watkins, Phys. Rev. B 2 (1970) 2859.
[38] S.M.A.M. Bouwens, D.C. Koningsberger, V.H.J. de Beer, S.P.A. Louwers and R. Prins, Catal. Lett. 5 (1990) 273.
[39] C.A. Muryn, D. Purdie, P. Hardman, A.L. Johnson, N.S. Prakash, G.N. Raikar, G. Thornton and D.S.-L. Law, Farady Discuss. Chem. Soc. 89 (1990) 77.
[40] A. Bianconi, in: *X-Ray Absorption*, eds. D.C. Koningsberger and R. Prins (Wiley, New York, 1988) p. 573.
[41] B. Scheffer, N.J.J. Dekker, P.J. Mangnus and J.A. Moulijn, J. Catal. 121 (1990) 31.
[42] N.K. Nag, D. Fraenkel, J.A. Moulijn and B.C. Gates, J. Catal. 66 (1980) 162.
[43] (a) J.K. Nørskov, B.S. Clausen and H. Topsøe, Catal. Lett. 13 (1992) 1;
(b) J.A. Rodriguez, J. Phys. Chem. B 101 (1997) 7524.
[44] J.E. Huheey, *Inorganic Chemistry*, 3rd Ed. (Harper & Row, New York, 1983) pp. 377–378.
[45] C.P. Li and D.M. Hercules, J. Phys. Chem. 88 (1984) 456.